A homogenized formulation to account for sliding of non-meshed reinforcements during the cracking of brittle matrix composites: Application to reinforced concrete

Alain Sellier, Alain Millard

A homogenized formulation to account for sliding of non-meshed reinforcements during the cracking of brittle matrix composites : application to reinforced concrete

Alain Sellier[a,1], Alain Millard[b]

[a] *LMDC, Université de Toulouse, INSA/UPS Génie Civil, 135 Avenue de Rangueil, 31077 Toulouse cedex 04 France.*

[b] *CEA DEN/DANS/DM2S/SEMT/LM2S, bâtiment 607 - CEN Saclay 91191 Gif sur Yvette cedex*

Abstract

Non-linear finite element modelling of complex structures made of composites, such as reinforced concrete, remains a challenge because, until now, the only way to consider the important phenomenon of sliding between the reinforcements and the brittle matrix of the composite has been to mesh the reinforcements and their interfaces explicitly . This method is accurate but so expensive in terms of computational resources that only critical small elements of composites structures are modelled using it. To get around this limit, a method avoiding the meshing of composite reinforcements is proposed. It consists in treating the sliding between reinforcements and matrix with a differential formulation that provides the deformation of reinforcements directly as a continuous field superimposed to the displacement field of the matrix. The method needs a minor modification of the finite element code, which can take advantage of its analogy with the anisotropic thermal formulation. After the analytical presentation of the method, two theoretical cases of study are given to confront the results obtained with this method without meshing of reinforcements, with reference results obtained using a complete mesh of the matrix, reinforcements and interfaces.

Keywords: Concrete, Damage, Reinforcements, Cracking, Finite elements

Email addresses: alain.sellier@univ-tlse3.fr (Alain Sellier), alain.millard@cea.fr (Alain Millard)

[1] Corresponding author

1. Introduction

Context. In civil engineering applications, crack opening in reinforced elements is a limit state to be controlled [44], because cracks are privileged ways for the ingress of deleterious agents. For instance, water and carbonic gas ingress rapidly in cracks and cause corrosion of the reinforcements. In other structures, such as water tanks and nuclear containment vessels, cracks opening is forbidden in normal conditions of exploitation, and when cracks occur in accidental conditions, the leakage flow must be limited to avoid dissemination of dangerous elements into the environment. So, predicting the crack opening and permeability of such structures is an objective for engineers dealing with these problems. Although progress has been made in recent decades to link crack opening and leakage flow [12, 31, 32, 30], the problem of crack opening assessment is still a major concern [36, 24].

Problem to solve. This problem is difficult to solve for two main reasons: the concrete has weak and relatively random tensile strength [35, 3] , and the reinforcements slide relatively to the concrete matrix during the formation of cracks [2, 13, 25]. The randomness of concrete tensile strength can be treated using various methods that are usable at different scales of modelling [43, 39, 4] but the sliding between reinforcements and the matrix can be treated only at the scale of the reinforcements, meshing them and their interfaces with the matrix explicitly [13, 6, 17, 22, 23] in order to consider the behavior law of the interface in the structural model. The consequence, in terms of computational resources, is problematic because, in the context of finite element modelling, the mesh size becomes controlled by the size of, and the spacing between, reinforcements, which leads to a number of nodes proportional to the size of the structure and prevents the use of large elements for large structures. For instance, the most complex numerical models currently used for a nuclear power plant containment vessel of more than 30 m diameter need to mesh all the reinforcements and pre-stressed wires. The spacing between reinforcements and wires being only a few decimeters, the finite element dimensions should be constrained to this size and, consequently, the number of finite elements will be far too high for engineering applications. So, to simplify the problem, the mesh is generally composed of larger finite elements, and kinematic relations between nodes of massive finite elements and nodes of segments used to mesh reinforcements are used. These kinematic relations assume a perfect bond between the reinforcements and the concrete, so, even if all the reinforcements are meshed [1, 5], the crack prediction is still not accurate because possible sliding between the two components is neglected. Until a method is found to consider the interaction between reinforcements and matrix in a very simple way, it will be difficult to improve the realism of models. That is our reason for proposing the present method.

Principle of the proposed method. This method is able to consider the sliding between reinforcements and the brittle matrix without meshing the reinforcements and their interfaces. It is based on the classic principle that the reinforced matrix can be modelled at large scales by a homogenized behavior law mixing the contributions of matrix and reinforcements. However, unlike classic homogenization methods, which consider reinforcements as inclusions in a representative elementary volume, the present method takes advantage of the finite element context to use a non-local formulation to assess reinforcements deformations, taking not only the sliding within but also outside the representative elementary volume into account. That is its main specificity. Finally, the strains in reinforcements are modelled using a continuous field that does not need the reinforcements to be meshed. Only their local volumetric fractions and their orientations are needed. These can be supplied to the finite element code as material parameter fields, independently of the underlying mesh. The paper first presents the theory of this method, then two virtual applications allow the method solution (coarse mesh without meshing of reinforcements) to be confronted with a reference solution obtained with a fine mesh including reinforcements and their interfaces.

2. Theoretical background

2.1. Equilibrium equation of a reinforcement

The local equilibrium of a cylindrical reinforcement section illustrated in Figure 1, along the local x axis, can be written:

$$\frac{\partial \sigma^r}{\partial x}\frac{\pi (D^r)^2}{4} + \tau^{m/r} \pi D^r = 0 \qquad (1)$$

with σ^r the axial stress in the reinforcement, D^r its diameter and $\tau^{m/r}$ the shear stress applied by the matrix on the reinforcement along the interface.

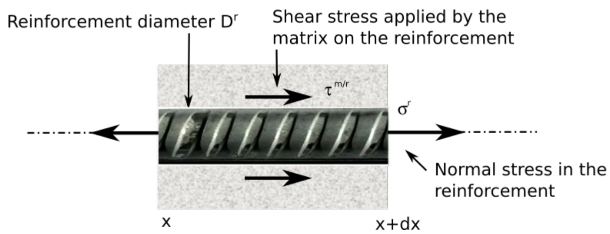

Figure 1: Axial and shear stresses applied to a reinforcement imbedded in a matrix

2.2. Behavior law of the reinforcement

The stress in the reinforcement is assumed to be coaxial with x, so its behavior law can be summed up in (2).

$$\sigma^r = E^r \underbrace{(\epsilon^r - \epsilon^{ra})}_{\epsilon^{re}} \tag{2}$$

with E^r the Young's modulus of the reinforcement, ϵ^{re} its elastic strain, ϵ^r its axial strain and ϵ^{ra} its an-elastic axial strain including plastic, visco-plastic [10] and thermal strain.

2.3. Bahavior law of the interface

In (1), the shear stress $\tau^{m/r}$ along the interface is assumed to depend only on the relative axial displacement $g^{m/r}$ between the matrix and the reinforcement (3).

$$\tau^{m/r} = K^i(g^{m/r} - g^{m/r\ a}) \tag{3}$$

with K^i the stiffness of the interface, $g^{m/r}$ the relative axial displacement between matrix and reinforcement, and $g^{m/r\ a}$ the an-elastic relative displacement. The behavior law of interface (3) is usually identified with a "pull-out" test [15] such as that illustrated in Figure 2.3. This figure is an illustration of a typical pull-out test obtained with a notched bar. Practically, the shape of the curve can be modified according to the material characteristics, bar diameter or notch height. The behavior law can also be expressed incrementally using the tangent stiffness H^i:

$$d\tau^{m/r} = H^i dg^{m/r} \tag{4}$$

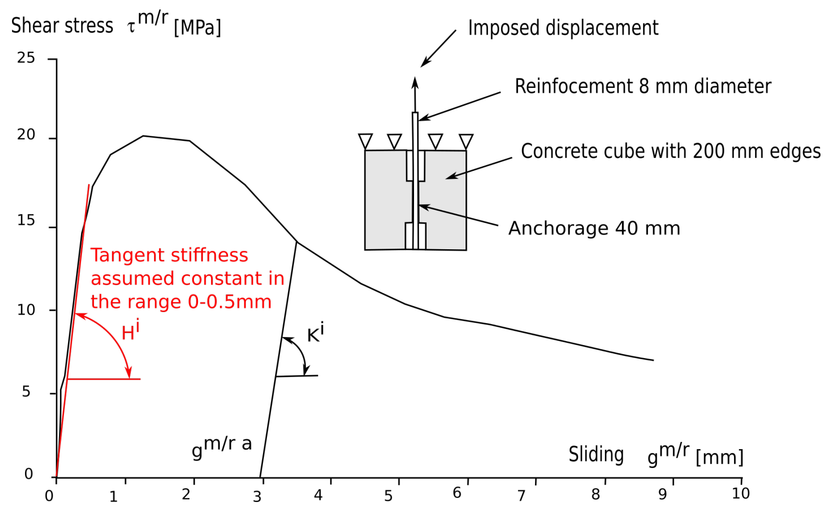

Figure 2: Interface behavior law identified with a pull-out test performed by N.Handika on steel rebar diameter 8 mm with lugs imbedded of 40 mm in a concrete block of 200 mm edges. The concrete characteristic were $Rc = 56MPa, Rt = 3.9MPa, E = 38500MPa$, [18]

2.4. Application domain

For the case of steel bars for reinforced concrete with lugs, according to experimental results shown in Figure 2.3, the initial tangent stiffness H^i can be kept constant until sliding reaches around 500 μm. This approximation can be exploited to simplify the numerical implementation of the non-local behavior law as explained below, but can also be avoided using an updating process of H^i in the numerical model. However, for the sake of simplicity, the non-local formulation is clarified below with the assumption of a constant tangent stiffness, H^i, that limits its current application domain to the sliding range $[0 - 500\ \mu m]$ in case of application to reinforced concrete. It is worth noting that a sliding of $[0 - 500\ \mu m]$ corresponds to the half crack opening (cf. Figure 3), the maximal crack opening conceivable with the simplified formulation is then 1 mm. This is sufficient for most reinforced concrete applications because the serviceability limit state is usually below 300 μm [11], and the ultimate state corresponds to the reinforcement plasticity, which generally occurs under 1 mm of crack opening. For other materials, such as carbon fiber composites or fiber concrete, the validity domain of this approximation will have to be defined before any application.

2.5. Kinematic equation

In a multi-cracked matrix, the sliding is maximal at the crack location and decreases with the distance from the crack until the symmetry plane as shown schematically in Figure 3. So, the sliding at the location of the crack can then be computed as the integral of difference in axial strains between reinforcement and matrix (5) from a symmetry plane between two cracks ($x = 0$).

$$g^{m/r}(x) = \int_{\xi=0}^{x} (\epsilon^m - \epsilon^r) d\xi \tag{5}$$

with $x = 0$ at the symmetry plane in Figure 3, and $x = x^c$ at the crack location relative to the symmetry plane.

2.6. Resulting differential formulation

In order to obtain a simple formulation combining the equilibrium equation (1), the behavior equations of the reinforcement (2) and of the interface (4), and the kinematic relation of sliding (5) in its derivative form, the equilibrium equation can be derived with respect to x and combined with the differential formulations of the behavior laws (6).

$$\begin{cases} \dfrac{\partial^2 \sigma^r}{\partial x^2} \dfrac{D^r}{4} + \dfrac{\partial \tau^{m/r}}{\partial x} = 0 \\ \dfrac{\partial^2 \sigma^r}{\partial x^2} = E^r \dfrac{\partial^2 \epsilon^{re}}{\partial x^2} \\ \dfrac{\partial \tau^{m/r}}{\partial x} = H^i \dfrac{\partial g^{m/r}}{\partial x} \\ \dfrac{\partial g^{m/r}}{\partial x} = \epsilon^m - (\epsilon^{re} + \epsilon^{ra}) \end{cases} \tag{6}$$

Once combined, the set of equations (6) leads to the resulting form (7).

$$\epsilon^{re} - \frac{E^r D^r}{4H^i} \frac{\partial^2 \epsilon^{re}}{\partial x^2} = \epsilon^m - \epsilon^{ra} \tag{7}$$

In (7), the elastic strain in the reinforcement (ϵ^{re}) appears to be the result of a second order differential equation in space analogous to the classical Helmholtz equation form (8). This type of equation is sometimes also used in mechanics to regularize finite element problems for which the material behavior law presents a softening leading to a crack localization [28, 26]. In this case, the Helmholtz form, also known as "second gradient formulation" or

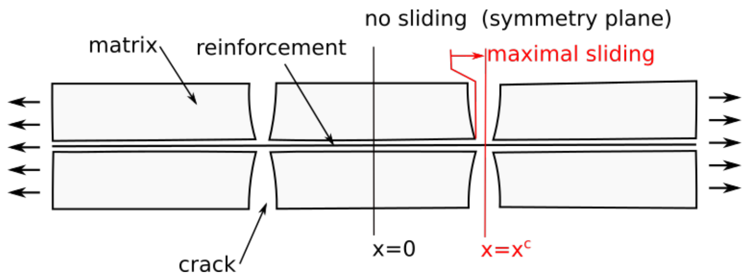

Figure 3: Crack periodicity, symmetry plane and maximal sliding at the crack tips

"phase field formulation" of the "non local theory", allows the internal variables controlling the softening to be spread over a zone that is independent of the finite element sizes. Another application of the Helmholtz equation is proposed in [39] to consider the Weibull scale effect in a simplified way. Equation (7) then constitutes the third application of this type of equation in solid mechanics.

$$\epsilon^{re} - \frac{l_c^{r^2}}{2} \frac{\partial^2 \epsilon^{re}}{\partial x^2} = S \tag{8}$$

In (8), l_c^r is a characteristic diffusion length and S is a source term. The analogy between (7) and (8) leads to the identification of these terms. The characteristic lenght l_c^r is given by (9), and the source term by (10).

$$l_c^r = \sqrt{\frac{E^r D^r}{2H^i}} \tag{9}$$

$$S = \epsilon^m - \epsilon^{ra} \tag{10}$$

With this formulation the elastic strain in the reinforcement appears analogous to the diffusion of the term $(\epsilon^m - \epsilon^{ra})$. It is worth noting that as long as $\epsilon^{ra} = 0$, the over-tension in the reinforcement due to the sliding is analogous to the diffusion of the strain ϵ^m in the finite element where the crack occurs. In other words, the sliding displacement along the rebar can be seen as a "diffusion" of the crack displacement jump over a length controlled by l_c^r.

2.7. Boundary conditions

Concerning the boundary conditions, if there is no sliding on the edges $\partial\Omega$ of the integration domain Ω (perfect anchorage at the edges), a Neumann condition can be used for the state variable ϵ^{re} (11).

$$\frac{\partial \epsilon^{re}}{\partial x} = 0 \text{ if } x \in \partial\Omega \tag{11}$$

In fact putting this condition into (8) leads to (12).

$$\epsilon^{r} = \epsilon^{m} \text{ if } x \in \partial\Omega \tag{12}$$

If (12) is true, it means that strains are the same in the matrix and the rebar, and there is then no sliding. Other types of boundary conditions may be used. For instance, to simulate a pull out, a Dirichlet condition could be used for ϵ^{re}, but, for the sake of simplicity, the applications below use only condition (12). In fact, the null Neumann boundary condition is the default condition of any formulation in the finite element codes, so this condition does not need to be specified in the code. This condition is realistic for some problems where sliding does not occurs perpendicularly to the edges. Specifically if the edges are free of stresses or weakly loaded, or subjected to imposed displacements.

3. Implementation in a finite element code to model reinforced brittle matrix

The interest of the differential form of the sliding reinforcement problem lies in its ability to be used in homogenized behavior laws of composites. Instead of meshing all the reinforcements, the interfaces and the matrix, the reinforcement elastic strain is treated as a diffuse field superimposed on the displacement field. To take advantage of this method, the finite elements code must be modified to be able to treat the two fields simultaneously. On the one hand, the equilibrium of the homogenized material has to be considered, and, on the other hand, the Helmholtz formulation provides the elastic strain of reinforcements. Once the two fields are known, the displacement field provides the matrix strains ϵ^{m} and the stresses in the matrix, while the field of ϵ^{re} enables the stresses field in the reinforcements to be computed.

3.1. Equations to be solved

The main balance equations to be solved are summarized below. The main state variables are the displacement $\vec{U}$ and the elastic strains in reinforcements ϵ^{re}_{n}, with ’n the reinforcement number. They are solved by the balance equations. Next, the state laws (behavior laws and evolution laws to account for non-linearities) can be used to assess the internal variables and stresses.

3.1.1. Balance equations

Two types of equilibrium equations have to be solved simultaneously:

- The classical stresses balance at the scale of the homogenized material (13). At this scale, the stresses are σ_{ij}, with i, j the subscripts corresponding to the global system coordinates and f_i the volume force in direction x_i.

- The shear stress balance at each interface between the matrix and a given reinforcement considered by (8).

These two sets of equations are summarized in (13).

$$\begin{cases} \displaystyle\sum_{j=1}^{3} \frac{\partial \sigma_{ij}}{\partial x_j} + f_i = 0 \text{ for } i \in [1, 2, 3] \\ \epsilon_n^{er} - \dfrac{l_{c_n}^{r^2}}{2} \dfrac{\partial^2 \epsilon_n^{er}}{\partial x_n^2} = S_n \text{ for } n \in [1..N^r] \end{cases} \tag{13}$$

In (13) N^r is the number of reinforcement types considered in the homogenized behavior law clarified below, x_n is the local coordinate along the reinforcement number n, and ϵ_n^{er} is the axial elastic deformation of a reinforcement.

3.1.2. State laws for each phase of composite

The state laws include the behavior law of the matrix, the behavior law of the reinforcements and the method for combining the stresses deduced from these two. A brief presentation of these three aspects of the homogenized behavior law is given below for reinforced concrete.

Homogenized stresses in the composite. The homogenized behavior law can be obtained using different homogenization methods, but, for the sake of simplicity, the simplest combination is used in the following. The homogenized stress σ_{ij} is simply obtained by summing of the matrix contribution and reinforcements contributions (14).

$$\sigma_{ij} = (1 - \sum_{n=1}^{N^r} \rho^n) \sigma_{ij}^m + \sum_{n=1}^{N^r} \rho^n \sigma_{ij}^{rn} \tag{14}$$

In (14), ρ^n is the volumetric fraction of reinforcement number n, σ_{ij}^m the stress in the matrix and σ_{ij}^{rn} the tensor component obtained with the reinforcement stresses (2) multiplied by the orientation tensors $\bar{\bar{P}}^{rn}$ (15).

$$P_{ij}^{rn} = e_i^{rn} e_j^{rn} \tag{15}$$

In (15), e_i^{rn} is a component of the unit vector $\vec{e^{rn}}$ giving the orientation of the reinforcement in the matrix. Equation (15) does not not consider the reorientation of the force in the reinforcement due to the dowel effect occurring when a crack opens in a direction different than the reinforcements ones. This dowel effect could be added using a method to compute the real directions of the forces in the reinforcements crossing the cracks.[38]

Stresses in the matrix. For the matrix (stresses σ_{ij}^m in (14)), the behavior law is derived from a model already described in [37]. It is a law based on plasticity and anisotropic damage. This law allows the softening behavior of the matrix to be considered. The fracture energy is managed using a local method derived from the Hillerborg principle [19]: in each principal direction of stresses in the matrix $\vec{e}_I$, the dimension l_I of the finite element is assessed using coordinates of the finite element nodes and their interpolation functions [41], and the softening branch of the behavior law is automatically adjusted to ensure the energy dissipated will be equal to the imposed fracture energy G_f. As the model is anisotropic, the principal stresses are assessed in the principal directions of effective stresses ($\tilde{\sigma}$) (16).

$$\sigma_I^m = (1 - D^c)(\tilde{\sigma}_I^{m-} C_I^c + (1 - D_I^t)\tilde{\sigma}_I^{m+}) \tag{16}$$

In (16), $\tilde{\sigma}_I^{m-}$ stands for the negative principal effective stresses and $\tilde{\sigma}_I^{m+}$ for the positive principal effective stresses. The damage D^c stands for the micro-cracking effect on the concrete stiffness: $D^c \to 1$ if the matrix is totally crushed and $D^c = 0$ for the undamaged matrix. This damage is driven by the plastic strains ϵ_{ij}^{mpc} induced by the yielding of a Drucker Prager criterion [14]. In (16) D_I^t is the tensile localized damage in the principal direction I. This damage depends on the maximum values reached by principal values of the plastic strains ϵ_{ij}^{mpt} induced by the yielding of principal stress criteria in each principal direction of $\tilde{\sigma}^m$. The decomposition of the effective stress tensor or strain tensor into positive and negative parts is a classic way to properly consider the two types of cracking possible in concrete but other decompositions could be used [34, 9]. C_I^c is a crack re-closure function, which also depends on the plastic strain ϵ_{ij}^{mpt}. This function allows us, for an existing localized crack already re-closed, to consider that if the crack re-opens, the contacts disappear between its edges ($C_I^c \rightarrow 0$), while the contacts reappear progressively when the crack re-closes ($C_I^c \rightarrow 1$). This is due to the roughness of the crack faces, which induce a progressive recovery of stiffness under negative stresses [21]. The crack re-closure is controlled with a principal stress criterion while the corresponding principal plastic strain ϵ_I^{mpt} stays positive, but, when this strain becomes zero, the criterion is deactivated in this direction and only the Drucker-Prager criterion controls the negative principal stresses. The Drucker-Prager criterion is a shear criterion sensitive to hydrostatic pressure: it considers the effect of the tri-axiality of the stress state on the compressive strength. An example of a cyclic test including damage in tension, damage and plasticity in compression, and tensile crack re-closures is given in Figure 4. In this model, used to manage the cracking of the matrix, the crack opening (w_I) is included in the finite element displacement field [30]. This feature allows ϵ^m to be used directly in (10) as explained above . If the interpolation functions used in the finite element for the displacement are linear, the relationship between the crack opening and the strain in the finite element is approximated using the plastic strain ϵ_I^{mpt} (17).

$$w_I = \epsilon_I^{mpt} l_I \tag{17}$$

The link between the crack opening and the tensile damage is given by equation (18).

$$D_I^t = 1 - \left(\frac{w_I^k}{w_I^k + \max(w_I)} \right)^2 \tag{18}$$

In (18), w_I^k is a parameter linked to the fracture energy G_f. The link between w_I^k and and the fracture energy depends on the finite element size l_I in the principal direction of tension. The relationship between w_I^k, the fracture energy G_f, and the finite element length l_I, is given by equation (19).

$$G_f = l_I R^t \left(\frac{R^t}{2E^m} + w_I^k \right) \tag{19}$$

In (19), E^m is the Young's modulus of the matrix and R^t its tensile strength. This relationship is the consequence of the Hillerborg principle: the energy consumed by a crack propagation is surfacic [19], while the energy computed by the program is proportional to the volume of the damaged finite element,

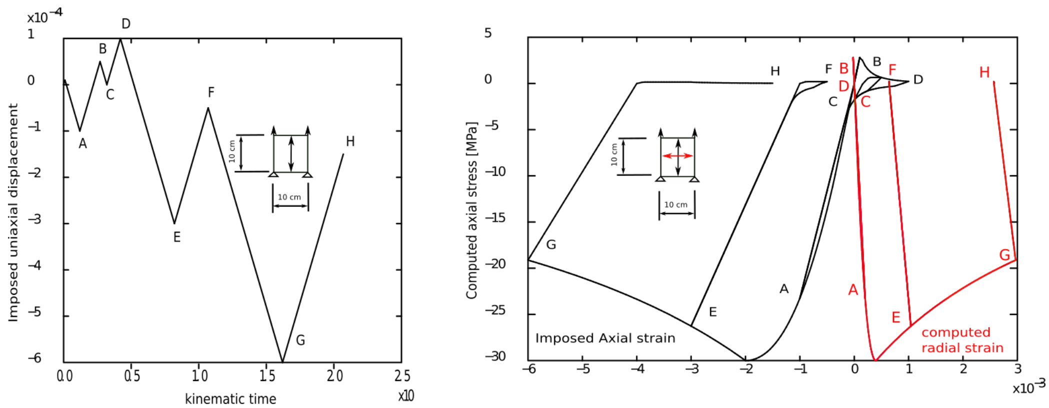

Figure 4: Matrix model response to a uniaxial cyclic test, for $E^m = 30GPa$, $R_c^m = 30MPa$, $R_t^m = 3MPa$, $G_f = 100J/m^2$, the finite element is a single cube having 10 cm edges.

so the volumetric energy has to be adapted (19) to satisfy the condition of equation (20).

$$G_f = l_I \int_0^\infty \sigma_I^m d\epsilon_I^{mpt} \tag{20}$$

Equation (20) shows that the element length (l_I) has to be assessed in the principal direction of the stresses in the matrix.

Stresses in the reinforcements. The behavior law for the reinforcements is elasto-plastic, with a kinematic linear hardening. The unixial behavior law is given by equation (2). It is also possible to take account of visco-plastic strain as explained in [10]. This feature is needed when dealing with pre-stressed wires, for example. For the sake of simplicity, this is not the case in the following applications.

3.2. Finite Element Formulation

As explained in the introduction, the objective is to avoid meshing the reinforcements with bars, interfaces, and so on. So the massive finite elements, used for the homogenized material, support both the displacement field and the elastic strain field of "distributed" reinforcements. For instance, in 3 dimensions, each node of the finite element model supports the state variables vector (21).

$$\begin{bmatrix} \begin{bmatrix} u \\ v \\ w \end{bmatrix} \\ \\ \begin{bmatrix} \epsilon_1^{er} \\ \dots \\ \epsilon_n^{er} \end{bmatrix} \end{bmatrix} \tag{21}$$

In (21), the first three variables are the displacements solved by the balance equations applied to the homogenized material, the last ones are the elastic strains of reinforcements, each one being solved by a Helmholtz equation corresponding to the condition of local equilibrium between matrix and reinforcements as explained above.

3.2.1. Variational form of Helmholtz equation

For a reinforcement oriented in a given direction x_n, the variational form of the Helmholtz equation (8) is written (22).

$$\int_\Omega \psi_n \epsilon_n^{er} dx_n - \int_\Omega \psi_n \frac{l_{c_n}^{r^2}}{2} \frac{\partial^2 \epsilon_n^{er}}{\partial x_n^2} dx_n - \int_\Omega \psi_n S_n dx_n = 0 \;\forall\; \psi_n \tag{22}$$

In (22), ψ_n is the test function. Using an integral transformation, this equation leads to the second variational form (23).

$$\int_\Omega \psi_n \epsilon_n^{er} dx_n - \left[\psi_n \frac{l_{c_n}^{r^2}}{2} \frac{\partial \epsilon_n^{er}}{\partial x_n} \right]_{\partial\Omega} + \int_\Omega \frac{\partial \psi_n}{\partial x_n} \frac{l_{c_n}^{r^2}}{2} \frac{\partial \epsilon_n^{er}}{\partial x_n} dx_n = \int_\Omega \psi_n S_n dx_n \;\forall\; \psi_n \tag{23}$$

with $\partial\Omega$ the edges of the meshed domain Ω.

3.2.2. Finite Element formulation

Taking the boundary conditions (11) into account, once discretized on the mesh and integrated over the whole structure by taking advantage of the finite element interpolation functions, the second form (23) becomes equivalent to the linear problem (24).

$$\underbrace{\left[\bar{\bar{C}} + \bar{\bar{K}}_n \right]}_{\bar{\bar{K}}_n^r} \epsilon_n^{\bar{er}} = \bar{S}_n^r \;\forall\; n \tag{24}$$

In (24) $\bar{\bar{C}}$ is a capacity matrix obtained by assuming a homogeneous unit capacity in the material, $\bar{\bar{K}}_n$ is an anisotropic conductivity matrix deduced from the equivalent material conductivity (25), and $\bar{S}_n$ is the source term re-assessed at each step of loading with (10). $\bar{\bar{K}}_n^r$ is the linear system resulting assembly of $\bar{\bar{C}}$ and $\bar{\bar{K}}_n$.

$$\bar{\bar{K}}_n = \frac{l_{c_n}^{r^2}}{2} \vec{e_n^r} \otimes \vec{e_n^r} \tag{25}$$

In (25) $\vec{e_n^r}$ is the local orientation of reinforcement number n. As the source term must be updated for each step of loading, the solving of (24) can be inserted in the global loop of non-linear-resolution of the finite element software: First the resolution of the equilibrium supplies the displacement increment field $(\Delta u, \Delta v, \Delta w)$, which is used to compute the strain increment in the matrix $\Delta\epsilon^m$, and the anelastic strain in the reinforcement ϵ_n^{ar} is initialized with the solution of the last converged step. These two terms are used to update the source term of (24). Once (24) is solved, the new elastic strain in the reinforcement (ϵ_n^{er}) is known and can be used to compute the stress in the reinforcement using (2). If plastic yielding occurs in the reinforcement, the source term is updated until convergence. Otherwise, the stress is directly used to compute the homogenized response of the material using equation (14). Finally at each sub-step of the non-linear procedure, the linear system to be solved is summarized in (26).

$$\begin{cases} \bar{\bar{K}} \Delta \bar{U} = \Delta \bar{F} \\ \Delta \bar{S}_n^r = \mathrm{sym}(\bigtriangledown(\Delta \bar{U})) - \Delta \epsilon_n^{\bar{r}a} \ \forall \ n \\ \bar{\bar{K}}_n^r \Delta \epsilon_n^{\bar{e}r} = \Delta \bar{S}_n^r \ \forall \ n \end{cases} \tag{26}$$

with $\bar{\bar{K}}$ the stiffness matrix of the structure, $\Delta\bar{U}$ the nodal increments of displacement, $\Delta\bar{F}$ the applied forces to be balanced (real forces increment for the first sub-step, or unbalanced internal forces during the iterative solving), $\mathrm{sym}(\bigtriangledown(\Delta\bar{U}))$ the symmetric part of the displacement increment gradient, and $\Delta\epsilon_n^{\bar{r}a}$ the an-elastic strain increment projected from the Gauss points to the nodes of the finite elements. This resolution method has been implemented in the finite element code Cast3m [7], in two steps at each iteration: first the equilibrium is solved to assess the displacement increments and strains, then the source term of the Helmholtz equation is deduced from the deformations and used to assess the elastic strain in the reinforcements. Once known, the stresses in the reinforcements and matrix are combined and the global equilibrium is tested. The procedure is iterated until the global equilibrium is verified.

4. Applications

First, two theoretical cases are treated in order to show the aptitude of the proposed method to consider correctly the linear de-bonding of a reinforcement in a simple reinforced concrete tie. Secondly a case of study is provided to illustrate the applicability of the method to a real structure with a more complex reinforcement system.

4.1. Theoritical cases

The objective of this section is to provide two elementary applications intended to test the numerical implementation of the method. First a simple reinforced concrete tie beam with a single crack is analyzed, then a second, longer tie with three cracks is studied.

4.1.1. Theoretical case with a single crack in a reinforced concrete tie beam

The first application concerns a theoretical reinforced concrete tie beam for which the homogenized finite element solution obtained with mesh (b) in Figure 5, is compared to a reference finite element solution obtained with the detailed mesh (a) in Figure 5. As can be observed in the Figure, the mesh (b) is simpler than (a) and number of nodes is considerably reduced. Even if each node of (b) supports the full state variables vector (21) instead of only the displacements, the computational duration is divided by 5, especially because the number of Gauss points where the behavior laws are integrated is reduced. And, in non-linear numerical models, more computational time is consumed for local non-linear behavior law solving (14) than for the linear resolution of the global system (24). The material characteristics of the reinforced concrete tie beam are given in Table 1. The tensile strength given in table 1 corresponds to the weakest zone. In the other zones of the tie the strength is three times higher to avoid any damage out of the predefined weakest zone. The interface stiffness given in table 1 is $40GPa$, it corresponds to a secant modulus of $300GPa$ in an interface zone $3mm$ thick with a Poisson coefficient $\nu = 0.25$. The reference solution is given in figure 6. It is Worth noting that this reference solution is based on two important assumptions: first the interface behavior is linear, secondly the concrete cracking is controlled using a Hillerborh method which considers the crack included in the finite

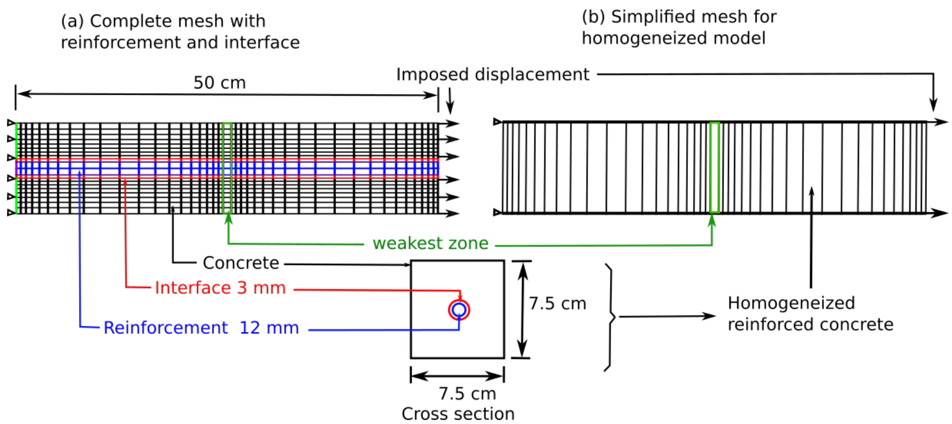

Figure 5: Complete mesh (a) and simplified mesh (b) for the single crack test

element, so that the strain in the finite element where the crack takes place, multiplied by the finite element length in the direction of crack opening, gives the crack opening, which is independent of the mesh size thanks to the Hillerborgh method. Due to this method, the finite element size where the crack takes place can be chosen freely. An interesting choice consists to adopt a dimension, for this finite element, close to the double of the length of the local conical failure of concrete occurring just around the crack. In fact, along this zone, the bond is damaged and the stress in the reinforcement quasi constant, what corresponds to the plateau observed in figure 6. This possibility is exploited in the current paper.

Reference solution compared to homogenized solution without the Helmholtz formulation. To show the efficiency of the proposed method, first the Helmholtz equation is switched off, so that the homogenized solution (mesh (b) in figure 5) considers a perfect bond between the reinforcement and the matrix, while the reference solution considers the possibility of sliding (mesh a). The reference solution is given in Figure 6. The cracking force is reached for point A in Figure 6 (a). The crack crosses the matrix section at point B. From B to C, the crack opens and sliding occurs. For each increment of imposed displacement, the stress profile along the reinforcement is plotted in Figure 6 (b). The stress concentration at mid length begins just after the crack propagation (between curves A and B), then the stress concentration increases until the end of loading (curve C). The solution obtained using a perfect

Table 1: Reinforced concrete tie beam material parameters

Parameter	Symbol	Value	Unit
Concrete parameters			
Young's modulus	E^m	30 000	MPa
Poisson's ratio	ν^m	0.2	–
Tensile strength in the weak zone	R_t^m	4	MPa
Compressive strength	R_c^m	57	MPa
Fracture energy	G_f^m	100	J/m^2
Reinforcement parameters			
Young's modulus	E^r	210 000	MPa
Elastic limit	f_y^r	500	MPa
Hardening modulus	H^r	1000	MPa
Interface parameters for mesh (a) in Figure 5			
Thickness	-	3	mm
Young's modulus	E^i	288	MPa
Poisson's ratio	ν^i	0.2	–
Interface parameters for mesh (b) in Figure 5			
Stiffness	H^i	40000	MPa/mm

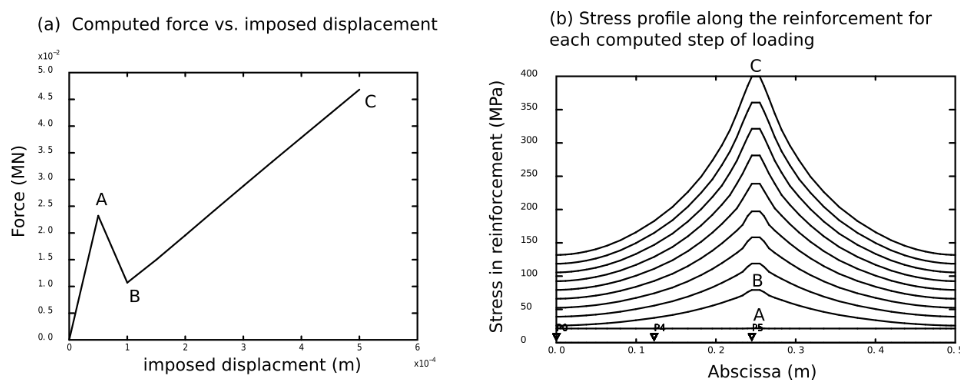

Figure 6: Reference solution (obtained with mesh(a) in Figure 5) for the tie beam with one crack: (a) force - displacement curve, (b) stress profile in reinforcement along the tie beam.

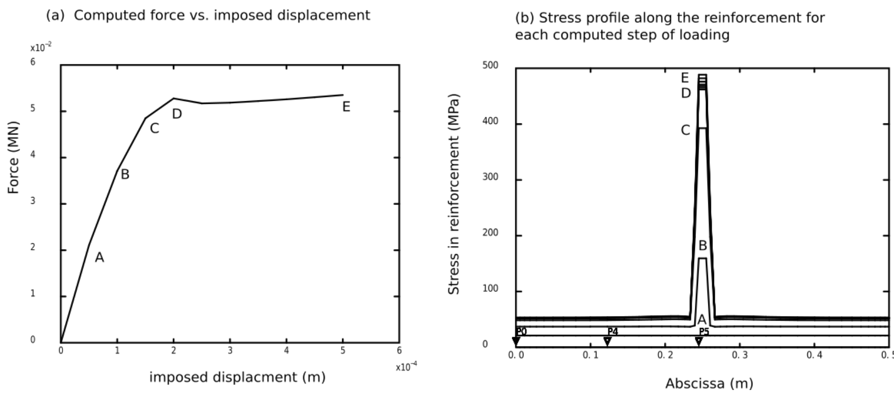

Figure 7: Solution with a perfect bond (obtained with mesh(b) in Figure 5) for the tie beam with one crack, (a) force - displacement curve, (b) stress profile in the reinforcement with the stress concentration in front of the crack.

bond between reinforcement and matrix is provided in Figure 7. As can be observed in 7 (a) the force-displacement curve presents greater stiffness than in Figure 6 (a). This can be explained by the greater increase of stress in the reinforcement in front of the crack. As, in this case, the reinforcement cannot slide, the reinforcement strain is concentrated in the finite element damaged by the localized crack. Consequently the strain increases faster and the plastic limit of reinforcement is reached at point D, while in the case with a possibility of sliding the plasticity of the reinforcement does not occur. This simple example shows how large the error on the assessment of a composite matrix can be when the sliding of reinforcement is neglected.

Reference solution compared to homogenized solution with Helmholtz formulation. A comparison of Figures 6 and 7 highlights the need to consider the interface behavior in a finite element analysis of composite material. The method used to consider the sliding allowed by the interface behavior led to a Helmholtz formulation that avoided meshing the reinforcement and the interface. This method, tested in the context of the homogenized formulation (14) uses the simplified mesh ((b) in Figure 5). The solution obtained is presented in Figure 8, where it is confronted with the reference solution. It is worth noting that the simplified solution is in good accordance with the reference one, showing that, in this case, the method based on the Helmholtz formulation is an interesting alternative to complete meshing, because it provides a very close solution for a reduced meshing and a reduced computational

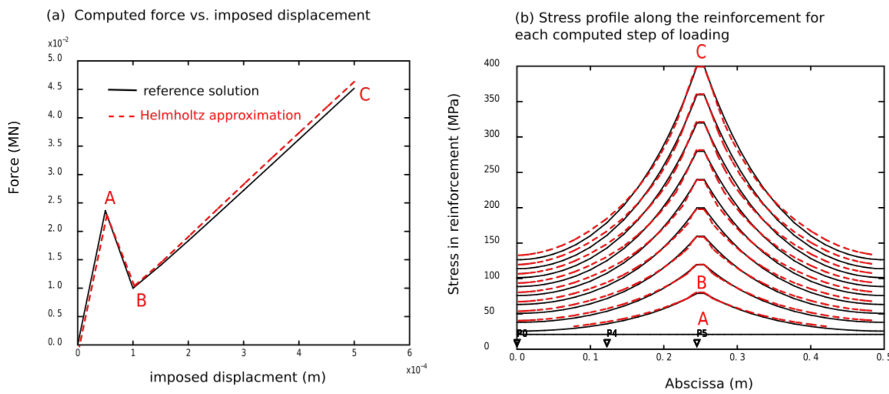

Figure 8: Comparison of the solution obtained with the simplified Helmholtz formulation (mesh (b) in Figure 5, dotted lines) with the reference solution (obtained with mesh(a) in Figure 5, plain lines) for the tie beam with one crack.

cost.

4.1.2. Theoretical case with several cracks in a reinforced concrete tie beam

To test the ability of the model to capture the complex phenomenon of multi-cracking, a second virtual study was carried out. It concerned a reinforced tie beam with the same cross section as in the previous case, but longer (1.5 m instead of 0.5 m), and with three prepositioned weak zones as represented and numbered in the diagram of Figure 9. All the other matrix reinforcement and interface characteristics were the same as specified in Table 1. The weakest zone is in the middle of the tie, with a strength $R_t^m = 4MPa$, the second weak zone is in the left part of the tie with a strength of $1.25R_t^m$, the third in the right part with a strength of $1.5R_t^m$. The rest of the tie has a strength of $3R_t^m$. The responses of the models are compared in Figure 10 in terms of force displacement and stress profiles along the reinforcement at different steps of loading. The Helmholtz results are also in good accordance with the reference solution. The cracks appear quasi simultaneously with those in the reference solution (for the same imposed displacements), and the stress levels in the reinforcement are relatively close. The small differences could be the consequences of differences of geometry: in the reference case the reinforcement was concentrated in the middle of the tie as shown in Figure 9(a) while the reinforcements are assumed to be distributed homogeneously in the cross section for the homogenization method (9(b)).

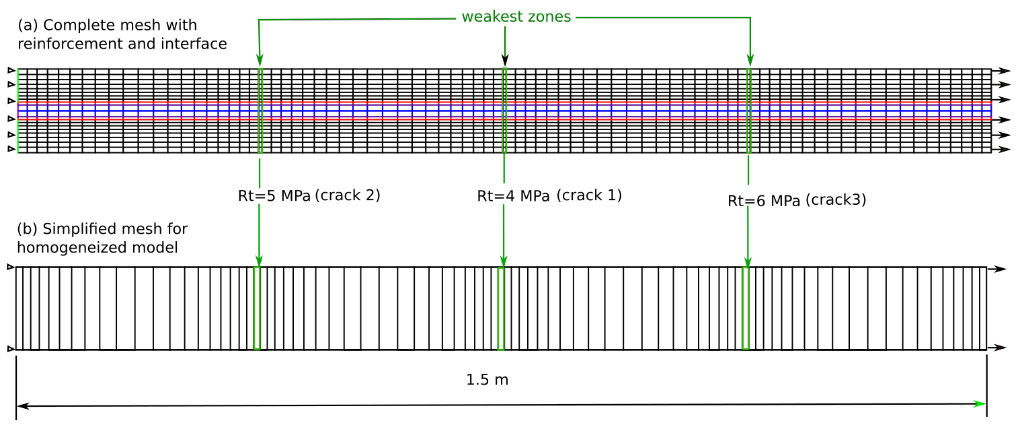

Figure 9: Meshes for the reference solution (a) with three cracks, and for the Helmholtz formulation (b)

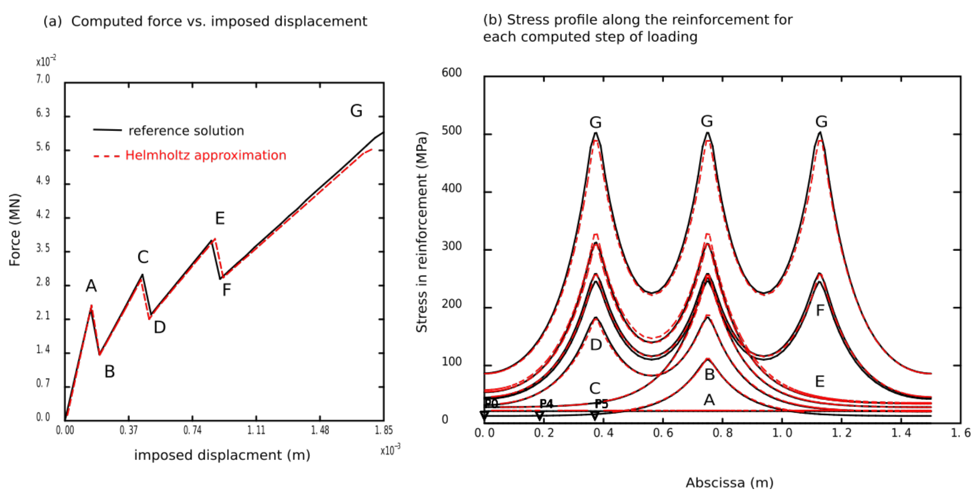

Figure 10: Comparison between the reference solution with three cracks, and the Helmholtz solution: (a) force displacement curves, (b) stresses in the reinforcement along the beam at different steps of loading.

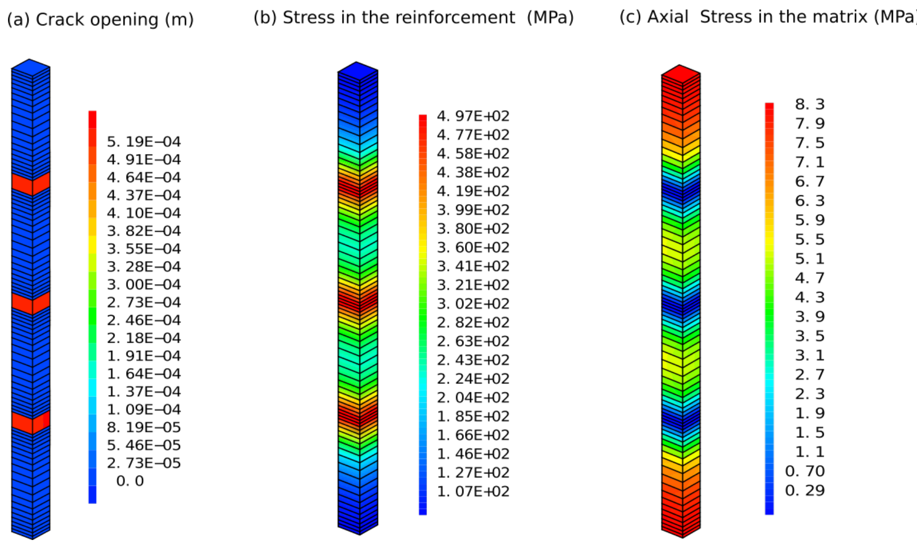

Figure 11: Illustration of results obtained with the homogenized model based on the Helmholtz formulation: (a) crack opening, (b) stress in the reinforcement, (c) stress in the matrix

To illustrate the fact that, in the case of the Helmholtz solution (homogenized material case), the stresses in the reinforcement are treated as continuous fields, like the stress in the matrix, Figure 11 shows the three major variables expected by the users for this type of modelling: the crack opening field, the stress in the reinforcement and the axial stress in the matrix.

4.2. Application to a real structure

The example chosen to illustrate the applicability of the method to a real structure is a reinforced concrete beam already widely studied by several authors in the framework of the French research project CEOS [8, 20].The geometry of the beam is given in Figure 13 and the material parameters in table 2. The mesh used is very simple, it is a regular distribution of cubic elements shown in figure 13, independent of the steel bars position and geometry. The reinforcements are not meshed but, in accordance with the proposed method, are considered only through their areas ratios and directions. In figure 13 the fields of reinforcement's area ratios are illustrated: the longitudinal re-bars are distributed in two zones, at the bottom and the top of the beam. The steel stirrups are considered also by this method with two other fields: one for the vertical parts of the frame and another one for the horizontal part. The size of these zones can be chosen relatively freely, the only condition to respect is that the total amount of reinforcement per zone must correspond to the real one. In this example the ratios and the directions are defined thank to parametric fields. The parameters of each field control the evolution of the fields versus the global coordinate system. So, to change the reinforcement's system, only the parameters of the fields would have to be changed. This method could be exploited to optimize positions, directions and ratios of reinforcements without changing the mesh. In figure 14, the computed force displacement curve is compared to the experimental one and to the results obtained with other classical models for which the reinforcements are explicitly meshed [20]. This comparison allows to verify that, despite the fact that reinforcements are not explicitly modelled, the stiffness loss due to the progressive cracking of the concrete, and the plateau of the curve predicted by the model, are close to the experimental ones and perfectly compatible with the other modellings of this beam. Figure 14 gives also the evolution of crack opening predicted by the model. It is worth noting that the beam presents a multi-cracking with numerous localized crack. Between 20 mm deflection and 30 mm deflection, the cracks number does not evolve but their openings increase due to the sliding of longitudianl and vertical reinforcements along the concrete. The longitudinal stress in concrete is illustrated in figure 15: In figure 15, the field SNC2 is the concrete stress in the axial direction. This stress reaches the compressive stress just under the point of applied load, leading to a crushing of concrete in this zone, which provokes a tensile stress in the upper part of steel stirrups (stress SNR1 in Figure 15, in the transverse direction). Despite the localized crack observable at mid span of the beam at the end of loading in Figure 14, the axial stress in the bottom reinforcements (SNR2 in Figure 15)is not localized, this is a consequence of sliding of these re-bars along the concrete in the vicinity of the localized cracks. Concerning stirrups, as their diameter is four time smaller than the longitudinal re-bars ones, their diffusion length (l_c in equation (9)) is then twofold smaller, and the stress field is less spreaded). It is also worth noting that the stress representation in figure 15 allows to control easily the stress levels in the different materials and the different directions, simply shifting from one internal variable of the model to another one.

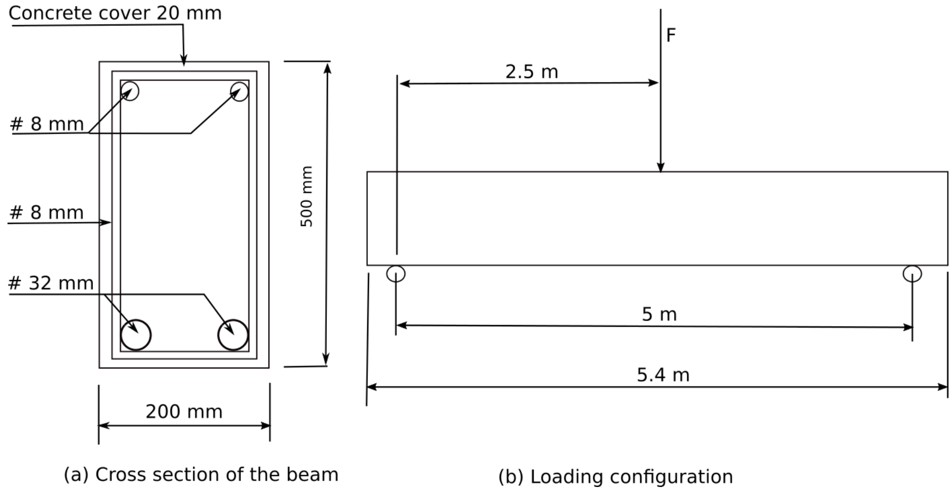

Figure 12: Reinforced concrete beam geometry

Table 2: Reinforced concrete beam material parameters

Parameter	Symbol	Value	Unit
Concrete parameters			
Young's modulus	E^m	37 200	MPa
Poisson's ratio	ν^m	0.27	–
Tensile strength in the weak zone	R_t^m	3.45	MPa
Compressive strength	R_c^m	36	MPa
Fracture energy	G_f^m	100	J/m^2
Reinforcement parameters			
Young's modulus	E^r	195 000	MPa
Elastic limit	f_y^r	466	MPa
Hardening modulus	H^r	3245	MPa

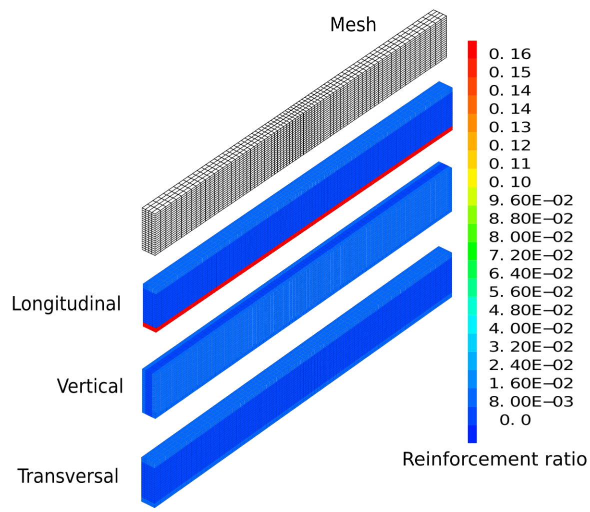

Figure 13: Reinforced concrete beam: Mesh and reinforcement ratio fields

5. Conclusion

To gain in efficiency and accuracy when calculating complex elements consisting of a mixed material combining a brittle matrix and oriented ductile fibers or reinforcements that may slip into the matrix during cracking, a non-local model of homogenized reinforcements has been developed. This model leads to the solving of a Helmholtz equation for each type of reinforcements. Once implemented in a finite element code, the Helmholtz equations avoid the need to mesh the reinforcements but enable their possible sliding to be considered, which plays an important role in the behavior of the cracked element. The paper gives the main equations and principles for the finite element implementation. It also provides the numerical solution of two theoretical tests, in order to verify that the implementation is correct. An application to a real reinforced concrete beam shows that this modelling method gives realistic responses, close to other classical models for which the reinforcement are explicitly meshed. Of course, other confrontations with experimental results will have to be done before applying the method to a real project. Perspective for continuing this work will be to improve the resolution algorithm and to extend the model to large crack openings, to cyclic conditions (for dynamic applications [34, 29]), to short fibers that may be totally pulled out during the crack opening [16], to evolutive matrices such

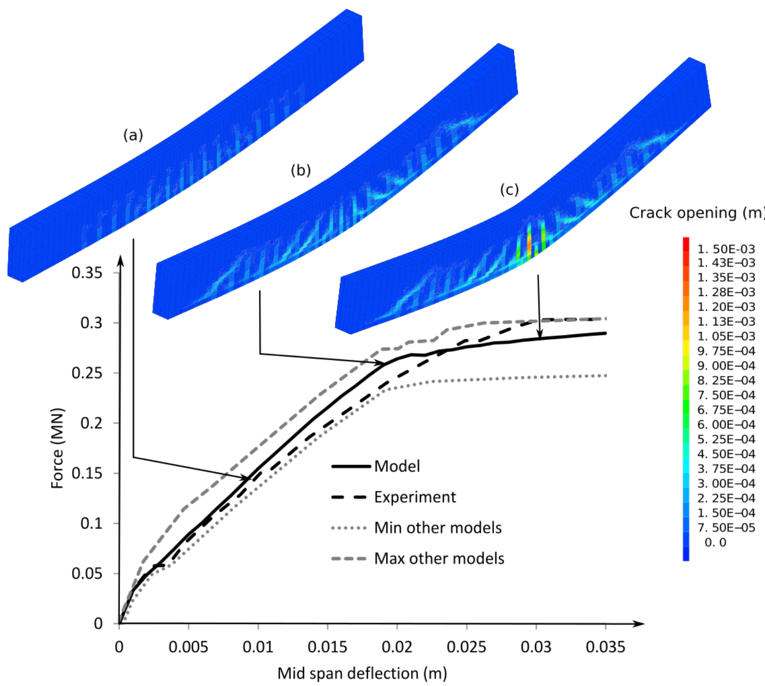

Figure 14: Force displacement curves, comparison model versus experiment, and computed crack opening [m] at different stages of loading: (a) 10 mm deflection, (b) 20 mm deflection, (c) 30 mm deflection. Min and Max of the other models come from the benchmark performed in the framework of the CEOS.fr research project [20].

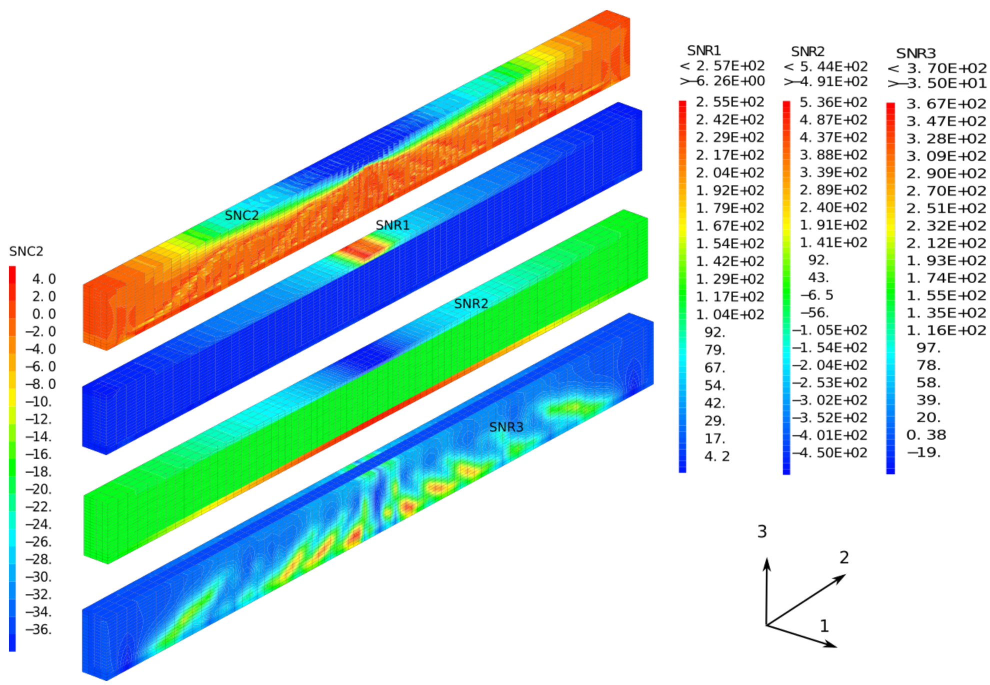

Figure 15: Computed stresses [MPa] at 30 mm deflection : SNC2 axial stress in concrete, SNR2 stress in distributed longitudinal reinforcements, SNR3 stress in distributed vertical reinforcements, SNR1 stress in distributed transversal reinforcements

as concrete affected by an alkali reaction [27] or delayed ettringite formation [42], and to problems of reinforcement corrosion [33]. Another perspective will be to consider the possible creep [40] of the interface when the loading is maintained for a long period.

Acknowledgements

The C.E.A (French Atomic and Alternative Energies Agency) is thanked for providing the finite element code Castem in its academic version. The ANR (French National Research Agency) is thanked for its contribution to the national research projects CEOS.fr and MACENA.

6. References

[1] Mehdi Asali, Bruno Capra, Jacky Mazars, and Jean-Baptiste Colliat. Numerical Strategy for Forecasting the Leakage Rate of Inner Containments in Double-Wall Nuclear Reactor Buildings. *Journal of Advanced Concrete Technology*, 14(8):408–420, 2016.

[2] Francis Barre, Philippe Bisch, Danièle Chauvel, Jacques Cortade, Jean-François Coste, Jean-Philippe Dubois, Silvano Erlicher, Etienne Gallitre, Pierre Labbé, Jacky Mazars, Claude Rospars, Alain Sellier, Jean-Michel Torrenti, and François Toutlemonde. *Control of Cracking in Reinforced Concrete Structures*. John Wiley & Sons, Inc., Hoboken, NJ, USA, 2016.

[3] Zdenk P. Bazant and Drahomir Novak. Probabilistic Nonlocal Theory for Quasibrittle Fracture initiation and size effect, I: Theory. *Journal of Engineering Mechanics*, (February):167–174, 2000.

[4] D.E.-M. Bouhjiti, J. Baroth, M. Briffaut, F. Dufour, and B. Masson. Statistical modeling of cracking in large concrete structures under Thermo-Hydro-Mechanical loads: Application to Nuclear Containment Buildings. Part 1: Random field effects (reference analysis). *Nuclear Engineering and Design*, 333:196–223, jul 2018.

[5] D.E.-M. Bouhjiti, M. Boucher, M. Briffaut, F. Dufour, J. Baroth, and B. Masson. Accounting for realistic Thermo-Hydro-Mechanical boundary conditions whilst modeling the ageing of concrete in nuclear contain-

ment buildings: Model validation and sensitivity analysis. *Engineering Structures*, 166:314–338, jul 2018.

[6] A. Casanova, L. Jason, and L. Davenne. Bond slip model for the simulation of reinforced concrete structures. *Engineering Structures*, 39:66–78, jun 2012.

[7] C.E.A. Cast3M : Finite Element Software, http://www-cast3m.cea.fr/, 2017.

[8] CEOS.fr. French National research project for design and assessment of special concrete structure toward cracking and shrinkage, 2009.

[9] Miguel Cervera, Claudia Tesei, and Giulio Ventura. Cracking of quasi-brittle structures under monotonic and cyclic loadings: A d+/d damage model with stiffness recovery in shear. *International Journal of Solids and Structures*, 135:148–171, mar 2018.

[10] Ponleu Chhun, Alain Sellier, Laurie Lacarriere, Sylvain Chataigner, and Laurent Gaillet. Incremental modeling of relaxation of prestressing wires under variable loading and temperature. *Construction and Building Materials*, 163:337–342, feb 2018.

[11] Code Model special activity group. Model Code 2010. Technical Report September, fib, CEB-FIP, 2011.

[12] C. Desmettre and J.-P. Charron. Water permeability of reinforced concrete with and without fiber subjected to static and constant tensile loading. *Cement and Concrete Research*, 42(7):945–952, jul 2012.

[13] Norberto Dominguez, Delphine Brancherie, Luc Davenne, and Adnan Ibrahimbegović. Prediction of crack pattern distribution in reinforced concrete by coupling a strong discontinuity model of concrete cracking and a bondslip of reinforcement model. *Engineering Computations*, 22(5/6):558–582, jul 2005.

[14] D. C. Drucker and W. Prager. Soil mechanics and plastic analysis for limit design. *Quarterly of Applied Mathematics*, 10(2):157–165, 1952.

[15] R Eligehausen, E.P Popov, and V.V Bertéro. Local bond stress-slip relationships of deformed bars under generalized excitations. In *Proceedings of the 7th European Conference on Earthquake Engineering. Vol. 4. Athens : Techn. Chamber of Greece*, pages 69–80, Athens, 1982.

[16] Rashid Hameed, Alain Sellier, Anaclet Turatsinze, and Frédéric Duprat. Metallic fiber-reinforced concrete behaviour: Experiments and constitutive law for finite element modeling. *Engineering Fracture Mechanics*, 103:124–131, may 2013.

[17] Rashid Hameed, Anaclet Turatsinze, Frédéric Duprat, and Alain Sellier. Bond stress-slip behaviour of steel reinforcing bar embedded in hybrid fiber-reinforced concrete. *KSCE Journal of Civil Engineering*, 17(7):1700–1707, nov 2013.

[18] Nuraziz Handika, Géraldine Casaux-Ginestet, and Alain Sellier. Influence of interface zone behaviour in reinforced concrete under tension : an analysis based on modelling and digital image correlation. In *Proceedings of the XIII International Conference on Computational Plasticity Fundamentals and Applications held in Barcelona, Spain 1-3 September 2015*, pages 122–133, Barcelona, 2015.

[19] A Hillerborg, M Modeer, and PE Peterssonn. Analysis of crack formation and crack growth in concrete by means of fracture mechanics and finite elements. *Cement and Concrete Research*, 6:773–782, 1976.

[20] Ludovic Jason. Rapport de recherche du PN CEOS : Axe Modélisation. Chargement statique monotone, rapport de synthèse du benchmark statique monotone. Technical report, CEA DM2S SEMT LM2S, Saclay, 2009.

[21] A. D. Jefferson and T. Bennett. Micro-mechanical damage and rough crack closure in cementitious composite materials. *International Journal for Numerical and Analytical Methods in Geomechanics*, 31(2):133–146, 2007.

[22] C Mang, L Jason, and L. Davenne. A new bond slip model for reinforced concrete structures : Validation by modelling a reinforced concrete tie. *Engineering Computations*, 32(7):1934–1958, 2015.

[23] Chetra Mang, Ludovic Jason, and Luc Davenne. Crack opening estimate in reinforced concrete walls using a steelconcrete bond model. *Archives of Civil and Mechanical Engineering*, 16(3):422–436, 2016.

[24] Mohammed Matallah and Christian La Borderie. 3D Numerical Modeling of the Crack-Permeability Interaction in Fractured Concrete. In V. Saouma, J. Bolander and E. Landis, editors, *Proceedings of the 9th International Conference on Fracture Mechanics of Concrete and Concrete Structures*, pages 1–8. IA-FraMCoS, 2016.

[25] A. Michou, A. Hilaire, F. Benboudjema, G. Nahas, P. Wyniecki, and Y. Berthaud. Reinforcement-concrete bond behavior: Experimentation in drying conditions and meso-scale modeling. *Engineering Structures*, 101, 2015.

[26] Gergely Molnár and Anthony Gravouil. 2D and 3D Abaqus implementation of a robust staggered phase-field solution for modeling brittle fracture. *Finite Elements in Analysis and Design*, 130(November 2016):27–38, 2017.

[27] Pierre Morenon, Stéphane Multon, Alain Sellier, Etienne Grimal, François Hamon, and Eric Bourdarot. Impact of stresses and restraints on ASR expansion. *Construction and Building Materials*, 140:58–74, 2017.

[28] HJ Peerlings, Ron. *Enhanced damage modelling for fracture and fatigue, ISBN 90-386-0930-2.* PhD thesis, Technische Universiteit Eindhoven, 1999.

[29] Frédéric Ragueneau and F Gatuingt. Inelastic behavior modelling of concrete in low and high strain rate dynamics. *Computers & structures*, 81(12):1287–1299, may 2003.

[30] S. Rahal and A. Sellier. Influence of crack reclosure on concrete permeability. *Theoretical and Applied Fracture Mechanics*, 100:65–77, apr 2019.

[31] S. Rahal, A. Sellier, and G. Casaux-Ginestet. Finite element modelling of permeability in brittle materials cracked in tension. *International Journal of Solids and Structures*, 113-114:85–99, may 2017.

[32] Giuseppe Rastiello, Stefano Dal Pont, Jean-Louis Tailhan, and Pierre Rossi. On the threshold crack opening effect on the intrinsic permeability of localized macro-cracks in concrete samples under Brazilian test conditions. *Mechanics Research Communications*, 90:52–58, jun 2018.

[33] Benjamin Richard, Sébastien Epaillard, Christian Cremona, Lennart Elfgren, and Lucas Adelaide. Nonlinear finite element analysis of a 50 years old reinforced concrete trough bridge. *Engineering Structures*, 32(12):3899–3910, dec 2010.

[34] Benjamin Richard, Frederic Ragueneau, Christian Cremona, and Lucas Adelaide. Isotropic continuum damage mechanics for concrete under cyclic loading: Stiffness recovery, inelastic strains and frictional sliding. *Engineering Fracture Mechanics*, 77(8):1203–1223, may 2010.

[35] P. Rossi, X. Wu, F. Maou, and A. Belloc. Scale effect on concrete in tension. *Materials and Structures*, 27(8):437–444, oct 1994.

[36] A. Sellier, G. Casaux-Ginestet, L. Buffo-Lacarrière, and X. Bourbon. Orthotropic damage coupled with localized crack reclosure processing. *Engineering Fracture Mechanics*, 97(January):168–185, jan 2013.

[37] A. Sellier, G. Casaux-Ginestet, L. Buffo-Lacarrière, and X. Bourbon. Orthotropic damage coupled with localized crack reclosure processing. Part I: Constitutive laws. *Engineering Fracture Mechanics*, 97(January):148–167, jan 2013.

[38] Alain Sellier. Anisotropic Damage and Visco-Elasto-Plasticity Applied to Multiphasic Materials. Technical report, Université de Toulouse, INSA, UPS, Toulouse, feb 2018.

[39] Alain Sellier and Alain Millard. Weakest link and localisation WL 2 : a method to conciliate probabilistic and energetic scale effects in numerical models. *European Journal of Environmental and Civil Engineering*, 18(10):1177–1191, apr 2014.

[40] Alain Sellier, Stéphane Multon, Laurie Buffo-lacarrière, Thierry Vidal, Xavier Bourbon, and Guillaume Camps. Concrete creep modelling for structural applications : non-linearity , multi-axiality , hydration , temperature and drying effects. *Cement and Concrete Research*, 79:301–315, 2016.

[41] Thomas Stablon, Alain Sellier, Nathalie Domede, Bernard Plu, and Luc Dieleman. Influence of building process on stiffness: numerical analysis of a masonry vault including mortar joint shrinkage and crack re-closure effect. *Materials and Structures*, 45(6):881–898, jun 2012.

[42] Yvan Thiebaut, Stéphane Multon, Alain Sellier, Laurie Lacarrière, Laurent Boutillon, Djemal Belili, Lionel Linger, François Cussigh, and Sofiane Hadji. Effects of stress on concrete expansion due to delayed ettringite formation. *Construction and Building Materials*, 183:626–641, sep 2018.

[43] J Van Mier. Influence of microstructure of concrete on size/scale effects in tensile fracture. *Engineering Fracture Mechanics*, 70(16):2281–2306, nov 2003.

[44] J Walvaren. Model Code 2010, final drafts. *FIB bulletin*, 1 & 2(65 & 56):105, 2012.